HoD–FP Algorithm for Unlimited Sensing: Where Time Meets Frequency

Conference Paper · September 2025

2 authors:

Ruiming Guo
Imperial College London

Ayush Bhandari
Massachusetts Institute of Technology

HoD-FP Algorithm for Unlimited Sensing: Where Time Meets Frequency

Ruiming Guo and Ayush Bhandari
Dept. of Electrical and Electronic Engg., Imperial College London, SW7 2AZ, UK.
{ruiming.guo,a.bhandari}@imperial.ac.uk

To Appear in the Proceedings of the 2025 IEEE International Workshop
on Computational Advances in Multi-Sensor Adaptive Processing

Abstract

Bridging the gap between theory and practice, the Unlimited Sensing Framework (USF) enables simultaneous enhancement of dynamic range and digital resolution within a fixed bit budget—an outcome unattainable with conventional sampling paradigms, which typically suffer from either signal clipping or loss of resolution. At the heart of USF lies non-linear folding in the analog domain, resulting in modulo samples and giving rise to a new class of signal recovery problems. In response, several time- and frequency-domain recovery algorithms have been proposed in recent years. In this work, we introduce a non-trivial hybridization that adopts a best of both (time-frequency) worlds approach, leading to the Higher-Order Fourier–Prony (HoD-FP) Algorithm. The HoD-FP not only refines the underlying sampling criteria but also achieves state-of-the-art signal recovery performance. We validate our method through different hardware experiments, demonstrating considerable reduction in sampling rate and dynamic range extension over existing techniques.

Index Terms

Analog-to-digital conversion, modulo non-linearity, sampling, signal sparsity, unlimited sensing framework.

CONTENTS

This work is supported by the EPSRC award no. EP/X040569/1, the ERC Starting Grant for "CoSI-Fold" (101166158) and the UKRI Future Leaders Program "Sensing Beyond Barriers via Non-Linearities" (MRC Fellowship award no. MR/Y003926/1). Further details on Unlimited Sensing and materials on *reproducible research* are available via `https://bit.ly/USF-Link`.

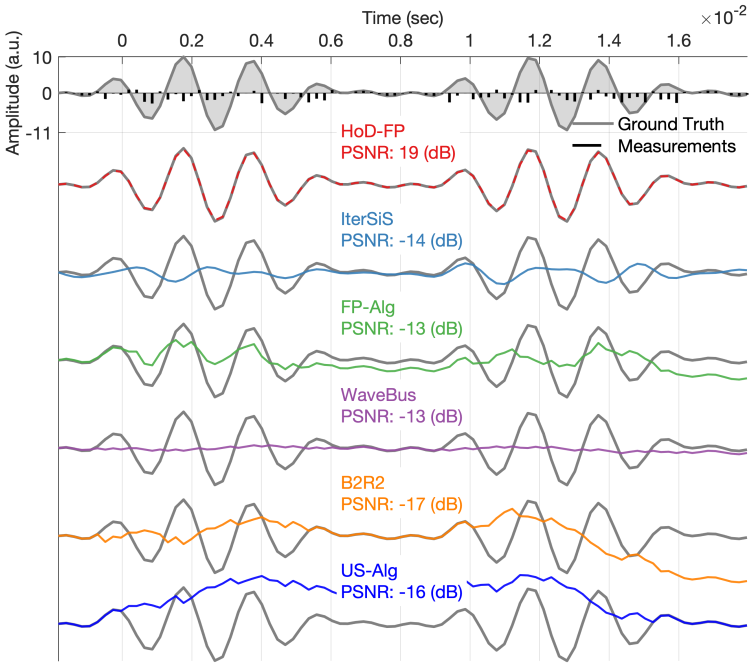

Fig. 1: Hardware Experiment: Extreme Sampling Conditions. We benchmark our HoD-FP method with existing approaches, including IterSiS [13], FP-Alg [3], WaveBus [14], B2R2 [15] and US-Alg [2]. We use the same signal waveform that was reported in Fig. 8 (Experiment 4) in [3], while pushing down the sampling rate as low as $3.42\times$ Nyquist-rate. Configured with $5.16\times$ dynamic range extension, this yields dense, closely-spaced folds ($M = 39$) in the measurements ($N = 89$), resulting in failures of existing approaches. Despite these algorithmic challenges, the proposed HoD-FP algorithm achieves accurate signal recovery using 6-th order difference, demonstrating its noise resilience and practical efficacy.

I. Introduction

The Unlimited Sensing Framework (USF) [1]–[3]. introduces a fundamentally new paradigm for analog-to-digital conversion (ADC), offering tangible advantages over conventional methods. What's radically different about USF? Any signal or sequence, say g, can be decomposed into an integer part (IP) or $\lfloor g \rfloor \in \mathbb{Z}$ and a fractional part (FP) or $[\![g]\!] \in [0,1)$:

$$\text{Signal} = \text{Integer Part} + \text{Fractional Part} \equiv g = \lfloor g \rfloor + [\![g]\!]$$

In engineering terms, the IP corresponds to the time- and amplitude-quantized digital signal, while the FP is typically regarded as undesirable quantization noise. USF pivots on a key mathematical insight: **for smooth signals, the fractional part encodes the integer part**. This redefines signal acquisition, representation and processing by enabling recovery of $\lfloor g \rfloor$ directly from sampled quantization noise, $[\![g]\!]$. Since the IP can be arbitrarily large ($\lfloor g \rfloor \propto g$), conventional ADCs face a fundamental constraint: with a fixed bit budget, one must choose between maximizing dynamic range (to avoid clipping) or achieving high digital resolution—but not both. In contrast, by digitizing only the FP or $[\![g]\!] \in [0,1)$—or equivalently, the modulo signal—USF eliminates this trade-off. This translates to simultaneous capture of high-dynamic-range (HDR) signal with high-digital-resolution (HDRes). The boost in HDRes implies higher data quality offering clear benefits for the recovery algorithms.

Starting with [3], the development of modulo ADCs [4]–[6] within the USF has led to both quantitative and qualitative performance upgrades, for instance, a 60x improvement in dynamic range [5]; a 10 dB reduction in quantization noise floor in radar [7] and tomography [8]; a 30 dB enhancement in Signal-to-Noise and Distortion (SINAD) [5]; support for higher-order modulation schemes in MIMO communications [9]; self-interference cancellation [10]; a 1200x downsampling factor in sub-Nyquist spectral estimation [11]; and improved signal and gesture classification accuracy [12].

Challenges and Related Works. Decoding the original HDR signal from the folded samples necessitates the novel mathematical algorithms. The existing approaches, also see Fig. 1, can be broadly categorized into two groups: 1) Time-domain approaches, starting with Unlimited Sampling algorithm (US-Alg) [1], [2], [4], linear prediction [16], unlimited one-bit (UNO sampling) [17], and WaveBus [14]. Such methods feature *DR compressibility* with recovery independent of the input DR *e.g.* US-Alg, and 2) Fourier-domain approaches such as the "Fourier–Prony" algorithm (FP-Alg) [3] leverage sparse priors. These methods exhibit noise resilience, but require a sampling rate that depends on the dynamic range (DR). Although FP-Alg delivers competitive performance, its sparsity assumption over modulo-induced folding limits DR compressibility, as the number of folds translates into unknown frequencies during parameter estimation.

Time-Frequency Hybridization Approach. Just as genetic hybridization yields advantageous traits by combining different gene pools, our algorithmic hybridization fuses time- and frequency-domain approaches to leverage complementary strengths for enhanced recovery performance. On one hand, higher-order differences (HoD) acting on $\lfloor g \rfloor$ in FP-Alg induce higher folds, increasing the number of unknown parameters and thus complicating the recovery problem. On the other hand, as shown in US-Alg, the same HoD operation is instrumental to the ethos of "unlimited sensing," enabling arbitrary HDR recovery. To construct a hybridized approach, we introduce HoD into FP-Alg. While this initially increases the parameter space, we mitigate the resulting complexity through non-linear filtering, by injecting the modulo operator into the recovery process. This reduces the effective number of unknowns while achieving HDR capabilities in FP-Alg that are otherwise unattainable with first-order differences alone.

Contributions. The core contribution of this work lies in the hybridization of US-Alg and FP-Alg, improving the sampling criteria and enabling performance improvement in sampling rate and dynamic range extension over existing approaches.

❏ **Algorithm.** We propose a novel recovery method, the HoD-FP, which generalizes the first-order FP-Alg and is backed by recovery guarantees, operating in regimes where existing methods fail (see Fig. 1).

❏ **Experiments.** We conduct hardware experiments under challenging scenarios—(i) 3.42x Nyquist rate, (ii) 11.24x DR extension, and (iii) 10.19 kHz input bandwidth—to demonstrate the practical advantages of the proposed HoD-FP method.

II. High-Order Fourier-Prony Recovery

Problem Formulation. We consider the τ-periodic bandlimited signal, which is mathematically defined as,

$$g(t) = \sum_{k=-K}^{K} g_k e^{\jmath \frac{2k\pi t}{\tau}}, \quad t \in [0, \tau], \quad g \in \mathbb{R} \tag{1}$$

for which its bandwidth is characterized by $\Omega_g = 2K\pi/\tau$. The folding non-linearity maps $g(t)$ into a low-dynamic-range, continuous-time signal, $y(t) = \mathscr{M}_\lambda(g(t))$, where

$$\mathscr{M}_\lambda : g \mapsto 2\lambda \left(\left[\!\left[\frac{g}{2\lambda} + \frac{1}{2} \right]\!\right] - \frac{1}{2} \right), \quad \begin{matrix} [\![g]\!] \stackrel{\text{def}}{=} g - \lfloor g \rfloor \\ \lambda > 0 \end{matrix} \tag{2}$$

and $\lfloor g \rfloor = \sup \{ k \in \mathbb{Z} | \, k \leqslant g \}$ denotes the integer part of g. Subsequently, $y(t)$ is pointwise sampled, resulting in folded samples $y[n] = \mathscr{M}_\lambda(g(t))|_{t=nT}, n \in \mathbb{I}_N$ where $T = \frac{\tau}{N}$ is sampling step and N is the number of samples ($\mathbb{I}_N = \{0, \ldots N-1\}$). In real-world scenarios, since the modulo-folding acts in analog-domain, noise arises from (i) thermal noise that follows a Gaussian distribution [18] and (ii) quantization noise that follows a uniform distribution. As a result, the noisy, "distorted" folded measurements can be expressed as [19], $y_w[n] = y[n] + w[n]$. In practice, since USF offers HDRes with the same bit-budget, thermal noise dominates the measurement noise, leading to $w[n] \sim \mathscr{N}(0, \sigma^2)$ [11]. We refer the reader to Fig. 6 in [11] for details on hardware experiments that justify the noise hypothesis. Given $\{y_w[n]\}_{n \in \mathbb{I}_N}$, our goal is to develop a *theoretically guaranteed recovery method* that is noise resilient and operates at *low-sampling-rate*.

Incorporating HoD with FP-Alg. The key advantage of FP-Alg lies in *enhancing sparsity* by using a combination approach: operating in HoD domain and introducing non-linear filtering. Note that, $g = \mathscr{M}_\lambda(g) + \varepsilon_g, \varepsilon_g(t) = \sum_{m=1}^{M} c_m u(t - \tau_m)$, where $u(\cdot)$ is the unit step function, and $c_m \in 2\lambda\mathbb{Z}$ and

$\tau_m \in T\mathbb{I}_N$ denote the fold amplitude and instant, respectively. Denote by $\{\Delta^{(h)}g, \Delta^{(h)}y, \Delta^{(h)}\varepsilon_g\}$ the h-th order finite difference of $\{g, y, \varepsilon_g\}$, respectively. Then, we have,

$$\Delta^{(h)}g\,[n] = \Delta^{(h)}y\,[n] + \Delta^{(h)}\varepsilon_g\,[n] \tag{3}$$

where $\Delta^{(h)}\varepsilon_g\,[n] = \sum_{m=1}^{M_h} c_{m,h}\delta\,[n - n_{m,h}]$, $c_{m,h} \in 2\lambda\mathbb{Z}$, $n_{m,h} \in \mathbb{I}_{N-h}$, and $M_h \geqslant M_{h-1}, h \in \mathbb{Z}^+$. While, in practice, the noisy folded measurements lead to, $\Delta^{(h)}y_w\,[n] = \Delta^{(h)}g\,[n] - \Delta^{(h)}\varepsilon_g\,[n] + \Delta^{(h)}w\,[n]$, where $\Delta^{(h)}w\,[n] \sim \mathcal{N}(0, \sigma_h^2)$ and $\sigma_h = (\frac{(2h)!}{(h!)^2})^{\frac{1}{2}}\sigma$. In this paper, we leverage the signal sparsity in HoD domain—an overlooked property in existing literature. By definition, we have,

$$\Delta^{(h)}g\,[n] = \mathscr{M}_\lambda(\Delta^{(h)}g\,[n]) + \varepsilon_{\Delta^{(h)}g}\,[n] \tag{4}$$

and from (3), using modular arithmetic, we can conclude that,

$$\mathscr{M}_\lambda(\Delta^{(h)}g\,[n]) \stackrel{(a)}{=} \mathscr{M}_\lambda(\Delta^{(h)}y\,[n]) \tag{5}$$

where (a) follows from $\Delta^{(h)}\varepsilon_g\,[n] \in 2\lambda\mathbb{Z}$. Hence, (4) translates to, $\Delta^{(h)}g\,[n] = \mathscr{M}_\lambda(\Delta^{(h)}y\,[n]) + \varepsilon_{\Delta^{(h)}g}\,[n]$, where

$$\varepsilon_{\Delta^{(h)}g}\,[n] = \sum_{m=1}^{\overline{M}_h} \overline{c}_{m,h}\delta\,[n - \overline{n}_{m,h}]\,, \;\; \overline{c}_{m,h} \in 2\lambda\mathbb{Z}. \tag{6}$$

Under appropriate sampling condition, we can obtain amplitude shrinkage of $\|\Delta^{(h)}g\|_{\ell_\infty}$, leading to *promotion of sparsity*,

$$\|\Delta^{(h)}g\|_{\ell_\infty} \leqslant \|\Delta^{(h-1)}g\|_{\ell_\infty} \implies \overline{M}_h \leqslant M_h. \tag{7}$$

Therefore, (7) enables the recovery of $\varepsilon_{\Delta^{(h)}g}$ via sparse estimation, so that $\mathscr{M}_\lambda(\Delta^{(h)}y\,[n]) + \varepsilon_{\Delta^{(h)}g}\,[n] \mapsto \Delta^{(h)}g\,[n]$.

Our main result is summarized as follows:

Theorem 1. *Let* $g\,(t) = \sum_{k=-K}^{K} g_k e^{\jmath\frac{2k\pi t}{\tau}}, t \in [0, \tau]\,, g \in \mathbb{R}$ *and the noisy folded samples be* $y_w\,[n] = \mathscr{M}_\lambda(g\,(nT)) + w\,[n]\,, n \in \mathbb{I}_N$ *with* $T = \tau/N$ *and* $w\,[n] \sim \mathcal{N}(0, \sigma^2)$. *Then,* $g\,[n]$ *can be reconstructed up to an error*

$$\mathsf{std}\{\mathcal{P}_{\frac{2K\pi}{\tau}}\,(\widetilde{g}) - g\} \leqslant \sqrt{\tfrac{2K}{N}}\sigma \tag{8}$$

where $\mathsf{std}\{\cdot\}$ *and* $\mathcal{P}_\Omega\,(\cdot)$ *represent the standard deviation and bandlimited projection within* $[-\Omega, \Omega]$*, provided that,*

$$\begin{aligned} &N \geqslant \max\left(\max\left(\tfrac{6\|g\|_{\mathbf{L}_\infty}}{\lambda}, 6K + 2\right) + h, \tfrac{2K\lambda^2(h!)^2}{\lambda^2(h!)^2 - 2\sigma^2(2h)!}\right), \\ &T < \tfrac{\tau}{4K\pi}, \;\; \textit{where} \;\; h = \left\lceil \tfrac{\ln(2\lambda) - \ln\|g\|_{\mathbf{L}_\infty}}{\ln(2K\pi T) - \ln\tau} \right\rceil. \end{aligned} \tag{9}$$

Proof. We start our proof with the amplitude shrinkage: Define the shift-difference operator as $\mathcal{S}_T\,(\cdot) = (\cdot)(t + T) - (\cdot)(t)$.

Amplitude Shrinkage. Then, by definition, we can derive that,

$$\Delta^{(h)}g\,[n] = \mathcal{S}_T^{(h)}\,(g)\,(t)\Big|_{t=nT}, \;\; \mathcal{S}_T^{(h)} = \mathcal{S}_T \circ \mathcal{S}_T^{(h-1)} \tag{10}$$

where $\circ$ denotes function composition. Next, we prove that $\|\mathcal{S}_T\|_{\mathbf{L}_\infty} < 1$ if $T < \frac{1}{\Omega_g}$. Since g is Ω_g-bandlimited, from Bernstein's inequality, we can derive that,

$$\|\mathcal{S}_T\,(g)\|_{\mathbf{L}_\infty} \leqslant \|\partial_t^{(1)}g\|_{\mathbf{L}_\infty}T \leqslant \Omega_g T\,\|g\|_{\mathbf{L}_\infty}\,.$$

By induction, we have $\left\|\Delta^{(h)}g\right\|_{\ell_\infty} \leqslant (\Omega_g T)^h \|g\|_{\mathbf{L}_\infty}$. Given $T < \Omega_g^{-1}$, hence, we can further derive that,

$$h \geqslant \left\lceil \frac{\ln(2\lambda) - \ln\|g\|_{\mathbf{L}_\infty}}{\ln(\Omega_g T)} \right\rceil \Longrightarrow \left\|\Delta^{(h)}g\right\|_{\ell_\infty} \leqslant 2\lambda. \tag{11}$$

Bounded Sparsity Level. Let $h = \left\lceil \frac{\ln(2\lambda) - \ln\|g\|_{\mathbf{L}_\infty}}{\ln(\Omega_g T)} \right\rceil$, then we can derive that, $\overline{M}_h \leqslant 4K$ since $\|\mathcal{S}_T^{(h)}(g)\|_{\mathbf{L}_\infty} \leqslant 2\lambda$ and thus the modulo-folding is only triggered when $|\mathcal{S}_T^{(h)}(g)(t)| \geqslant \lambda$.

Residue Estimation via Fourier Partitioning. Denote by $\{\widehat{g}_h, \widehat{y}_{h,w}, \widehat{\varepsilon}_{g,h}, \widehat{w}_h\}$ the Discrete Fourier Transform (DFT) of $\{\Delta^{(h)}g, \Delta^{(h)}y_w, \varepsilon_{\Delta^{(h)}g}, \Delta^{(h)}w\}$, respectively and,

$$\widehat{y}_{h,w}[l] \approx \widehat{g}_h[l] - \widehat{\varepsilon}_{g,h}[l] + \widehat{w}_h[l], \quad l \in \mathbb{I}_{N-h}. \tag{12}$$

To evaluate $\widehat{y}_{h,w}$, we first compute $\Delta^{(h)}g$, as well as $\widehat{g}_h$. By definition, from (1), we can obtain that,

$$\Delta^{(h)}g[n] = \sum\nolimits_{k=-K}^{K} g_{k,h} e^{\jmath\frac{2k\pi T n}{\tau}}, \; g_{k,h} = g_k(e^{\jmath\frac{2k\pi T}{\tau}} - 1)^h.$$

Then, $\widehat{g}_h[l]$ can be mathematically characterized as,

$$\widehat{g}_h[l] \overset{(b)}{\approx} \sum_{k=-K}^{K} g_{k,h} \sum_{n=0}^{N-h-1} e^{\jmath\frac{2\pi n}{N-h}(k-l)} = (N-h) g_{m,h}$$

which follows from the hypothesis that N is sufficiently large. As a result, we can derive that, $\widehat{g}_h[l] = 0, \forall l \in [K+1, N-h-K]$. Hence, in the out-of-band region ($[K+1, N-h-K]$), we have $\widehat{y}_{h,w}[l] = -\widehat{\varepsilon}_{g,h}[l] + \widehat{w}_h[l]$. Next, we compute $\widehat{\varepsilon}_{g,h}$ and $\widehat{w}_h$ to characterize $\widehat{y}_{h,w}$, utilizing (6),

$$\begin{array}{l} \widehat{\varepsilon}_{g,h}[l] = \sum_{m=1}^{\overline{M}_h} \overline{c}_{m,h} e^{\jmath u_{m,h} l}, \; \mathbb{E}\left((\widehat{w}_h)^2\right) = \sigma^2_{\widehat{w}_h} \\ \text{where } \; u_{m,h} = \frac{-2\pi \overline{n}_{m,h}}{N-h} \; \text{ and } \; \sigma_{\widehat{w}_h} = \left(\frac{(N-h)(2h)!}{(h!)^2}\right)^{\frac{1}{2}} \sigma \end{array}.$$

Note that, $\overline{c}_{m,h} \in \{-2\lambda, 2\lambda\}$ since $\|\mathcal{S}_T^{(h)}(g)\|_{\mathbf{L}_\infty} \leqslant 2\lambda$. Thus, in the out-of-band region, $\widehat{y}_{h,w}$ can be expressed as,

$$\widehat{y}_{h,w}[l] = \sum_{m=1}^{\overline{M}_h} -\overline{c}_{m,h} e^{\jmath u_{m,h} l} + \widehat{w}_h[l]. \tag{13}$$

Finding $\{\overline{c}_{m,h}, u_{m,h}\}_{m=0}^{\overline{M}_h - 1}$ from $\{\widehat{y}_{h,w}[l]\}_{l=K+1}^{N-h-K}$ boils down to spectral estimation. To establish the link between noise level and parametric estimation precision, we resort to the Cramér-Rao Bounds (CRBs) under additive white Gaussian noise $\widehat{w}_h$. As shown in [20]–[22], the CRBs derived for individual frequency apply to multiple frequencies scenario, if they are well-separated. Such kind of result holds in our context, since $\|\mathcal{S}_T^{(h)}(g)\|_{\mathbf{L}_\infty} \leqslant 2\lambda$. Let $\{\mathsf{std}\{\overline{c}_{m,h}\}, \mathsf{std}\{u_{m,h}\}\}$ represent the standard deviation of the error of estimating the sinusoidal parameter $\{\overline{c}_{m,h}, u_{m,h}\}$, thus the CRBs read [23], $\mathsf{std}\{u_{m,h}\} \geqslant \frac{\sqrt{6}\sigma_{\widehat{w}_h}}{|\overline{c}_{m,h}|(N-h-2K)^{3/2}}$, $\mathsf{std}\{\overline{c}_{m,h}\} \geqslant \frac{\sigma_{\widehat{w}_h}}{\sqrt{2}(N-h-2K)^{1/2}}$. It is well-documented that the accuracy of algorithms like maximum likelihood estimator asymptotically approach CRBs for a large range of noise levels, when the number of samples N tends to infinity [21], [24]. This suggests, if such efficient algorithms are used and N is sufficiently large, the inequality above can be treated as an equality in practice, leading to, $\mathsf{std}\{\overline{n}_{m,h}\} = \frac{\sqrt{6}(N-h)\sigma_{\widehat{w}_h}}{4\pi\lambda(N-h-2K)^{3/2}}$, $\mathsf{std}\{\frac{\overline{c}_{m,h}}{2\lambda}\} = \frac{\sigma_{\widehat{w}_h}}{2\sqrt{2}\lambda(N-h-2K)^{1/2}}$, where $\overline{n}_{m,h} \in \mathbb{I}_{N-h}$ and $\frac{\overline{c}_{m,h}}{2\lambda} \in \{-1, 1\}$, hence, we can exactly find $\{\overline{c}_{m,h}, \overline{n}_{m,h}\}$ if,

$$\max\left(\mathsf{std}\{\overline{n}_{m,h}\}, \mathsf{std}\{\tfrac{\overline{c}_{m,h}}{2\lambda}\}\right) \leqslant \tfrac{1}{4}. \tag{14}$$

Given that N is large enough, *i.e.* $N - h \gg 6K + 2$, we have $\mathsf{std}\{\overline{n}_{m,h}\} \leqslant \mathsf{std}\{\frac{\overline{c}_{m,h}}{2\lambda}\}$, and thereby, (14)

TABLE I: Hardware Experiments: Parameters and Performance Metrics.

Figure	Exp. No.	Oversampling Factor	$\frac{\Omega_g}{2\pi}$	T	$\|g\|_{\mathbf{L}_\infty}$	λ	N	M	h	$\mathcal{E}(\widetilde{\mathbf{g}},\mathbf{g})$				
			(kHz)	(μs)	(V)	(V)				HoD-FP	IterSiS [13]	FP-Alg [3]	WaveBus [14]	B2R2 [15]
Fig. 1	I	3.42	0.65	225	10.37	2.01	89	39	6	$\mathbf{1.40\times10^{-2}}$	2.31×10^{1}	1.86×10^{1}	2.01×10^{1}	4.89×10^{1}
—	II	6.45	1.11	70	8.99	0.80	400	205	4	$\mathbf{2.47\times10^{-2}}$	—	—	1.50×10^{1}	2.66×10^{1}
—	III	4.46	10.19	11	1.97	0.40	455	318	2	$\mathbf{1.41\times10^{-3}}$	—	—	1.37×10^{0}	1.54×10^{0}

translates to,

$$\sqrt{\tfrac{N-h}{N-h-2K}}\sqrt{\tfrac{(2h)!}{(h!)^2}}\frac{\sigma}{\lambda} \leqslant \frac{1}{\sqrt{2}}. \tag{15}$$

Since $\frac{N-h}{N-h-2K} < \frac{N}{N-2K}$, hence $\frac{N}{2K} \geqslant (1 - \frac{2\sigma^2}{\lambda^2}\frac{(2h)!}{(h!)^2})^{-1}$ guarantees that (14) holds, where $N/2K = \pi/\Omega_g T$ represents the oversampling factor. Hence, $\varepsilon_{\Delta^{(h)}g}$ can be recovered.

Recovery and Denoising. With $\varepsilon_{\Delta^{(h)}g}$ known, we can recover ε_g up to an unknown constant ($2\lambda\mathbb{Z}$) via anti-difference operation [2]. From (3) and (4), we obtain $\Delta^{(h)}\varepsilon_g$, since $\Delta^{(h)}\varepsilon_g[n] = \mathscr{M}_\lambda(\Delta^{(h)}y[n]) + \varepsilon_{\Delta^{(h)}g}[n] - \Delta^{(h)}y[n]$. Let S denote the anti-difference operator followed by on-grid projection, which is defined as, $\mathsf{S}\Delta^{(l)}\varepsilon_g \mapsto \left\lfloor \mathsf{S}\Delta^{(l)}\varepsilon_g + \lambda/(2\lambda)\right\rfloor$. This leads to $\Delta^{(l-1)}\varepsilon_g[n] = \mathsf{S}\Delta^{(l)}\varepsilon_g[n] + \kappa_l f[n]$, where $f[n] = 2\lambda$ and $\kappa_l \in \mathbb{Z}$. As demonstrated in [2], we can resolve $\kappa_l, l \in [2,h]$. By applying S twice, we have that,

$$\Delta^{(l-2)}\varepsilon_g[n] = \mathsf{S}^{(2)}\Delta^{(l)}\varepsilon_g[n] + \kappa_l\mathsf{S}f[n] + \kappa_{l-1}f[n] \tag{16}$$

where $\mathsf{S}f[n] = 2\lambda n$ is a linear sequence. Furthermore, $\left|\Delta^{(l-2)}\varepsilon_g[n] - \Delta^{(l-2)}\varepsilon_g[n+J]\right|$ is upper bounded, since

$$\Delta^{(l-2)}\varepsilon_g([n]-[n+J]) \in 2\lambda J\left[\kappa_l - \tfrac{3\|g\|_{\mathbf{L}_\infty}}{2\lambda J}, \kappa_l + \tfrac{3\|g\|_{\mathbf{L}_\infty}}{2\lambda J}\right]. \tag{17}$$

As a result, (17) has an unique integer solution to κ_l, if

$$\frac{3\|g\|_{\mathbf{L}_\infty}}{2\lambda J} \leqslant \frac{1}{4} \iff J \geqslant \left\lceil \frac{6\|g\|_{\mathbf{L}_\infty}}{\lambda}\right\rceil. \tag{18}$$

We refer the reader to Theorem 2 in [2] for mathematical details. With (17) and (18), we can recursively estimate κ_l and reconstruct ε_g and $\widetilde{g}$ up to an unknown constant $2\lambda\mathbb{Z}$,

$$\widetilde{g}[n] = y_w[n] + \mathsf{S}^{(h)}\Delta^{(h)}\varepsilon_g[n]. \tag{19}$$

The signal prior in (1) allows for enhancing reconstruction precision via low-pass filtering, which is, $\mathcal{P}_{\Omega_g}(g) = g$ and $\mathsf{std}\{\mathcal{P}_{\Omega_g}(w)\} = (\frac{2K}{N})^{1/2}\sigma$, where $\mathcal{P}_{\Omega_g}(\cdot)$ denotes the bandlimited projection within $[-\Omega_g, \Omega_g]$. Integrating ingredients above, finally we have, $\mathsf{std}\{\mathcal{P}_{\Omega_g}(\widetilde{g}) - g\} \leqslant (\frac{2K}{N})^{1/2}\sigma$. □

Remarks. The key takeaway from Theorem 1 is threefold: i) Theorem 1 improves the sampling rate condition in [2] by eliminating the Euler's constant "e", ii) Theorem 1 also applies to general bandlimited signals, although it is derived based on the signal model in (1) (see Section III), and iii) Oversampling factor, namely $\frac{N}{2K}$, affects the finite difference depth h and final recovery precision (8).

Algorithmic Implementation. The proof of Theorem 1 is constructive and leads to a noise resilient signal recovery approach—high-order Fourier-Prony algorithm (*viz.* HoD-FP), that also applies to general bandlimited signals. One key step in HoD-FP method is spectral estimation, aiming at finding the residue against amplified measurement noise. In this paper, we use the classic matrix pencil method for this purpose [25] [1]. The procedure of HoD-FP is summarized in Algorithm 1.

[1]Other high-resolution techniques like atomic-norm minimization [26] and model-fitting [24] could also be used in our context.

HoD-FP: High-Order Fourier-Prony Recovery.

Input: Noisy folded measurements $\{y_w[n]\}_{n\in\mathbb{I}_N}$.

1: Compute the difference order h via (11).
2: Conduct h-th order difference on y_w.
3: Calculate $\widehat{y}_{h,w}[l]$ via DFT.
4: Using matrix pencil [25] to recover $\varepsilon_{\Delta^{(h)}g}$.
5: Recover ε_g by recursively computing κ_l via (17).
6: Reconstruct $\widetilde{g}$ via (19).
7: Conduct bandlimited projection: $\widetilde{g} \leftarrow \mathcal{P}_{\Omega_g}(g)$.

Output: The recovered signal $\widetilde{g}$.

III. Experiments

To translate theory into practice, we conduct three hardware experiments to validate the proposed HoD-FP algorithm, spanning (i) low-sampling-rate, (ii) large dynamic range (DR) extension and (iii) large input bandwidth. We benchmark our method against existing recovery approaches, including IterSiS [13], FP-Alg [3], WaveBus [14] and B2R2 [15], to demonstrate its algorithmic robustness and practical advantages.

Experimental Protocol. In each experiment, the analog bandlimited signal generated from function generator is fed into modulo-ADC [3]. Together with the output of the modulo-ADC, we simultaneously record the original HDR input on the oscilloscope, serving as the ground truth. Experimental parameters including input bandwidth Ω_g, sampling rate T, dynamic range $\|g\|_{\mathbf{L}_\infty}$, among others are tabulated in Table I.

Low-Sampling-Rate. Oversampling is the critical factor for most USF recovery methods. In the first experiment, we use the same signal waveform that was evaluated in Fig. 8 (Experiment 4) in [3], while pushing the sampling rate as low as 3.42 Nyquist-rate with $5.16\times$ DR extension, as shown in Fig. 1. Due to the challenging sampling scenario, all existing approaches fail (see Fig. 1). However, our HoD-FP algorithm offers an accurate signal reconstruction with $\mathcal{E}(\widetilde{\mathbf{g}}, \mathbf{g}) \propto 10^{-2}$, operating at 6-th order difference domain. This effectively demonstrates the low-sampling-rate capability and noise resilience of the proposed HoD-FP method.

Large DR. Dynamic range and input signal bandwidth are the two key metrics to evaluate the performance of USF. To this end, in the second experiment, we increase the DR extension as $\|g\|_{\mathbf{L}_\infty}/\lambda = 11.24$ with oversampling factor of $\frac{\pi}{\Omega_g T} = 6.45$. This setting yields $M = 205$ folds out of 400 measurements, where the existing approaches [3], [13]–[15] cannot handle (*i.e.* $M > \frac{N}{2}$), as reported in Table I. While, our HoD-FP algorithm adopts 4-th order difference, and achieves precise signal reconstruction $\mathcal{E}(\widetilde{\mathbf{g}}, \mathbf{g}) \propto 10^{-2}$.

Large Input Bandwidth. In the last experiment, we further push the signal bandwidth to $\frac{\Omega_g}{2\pi} = 10.19$ kHz and use oversampling factor of $\frac{\pi}{\Omega_g T} = 4.46$ with $\|g\|_{\mathbf{L}_\infty}/\lambda = 4.93$. This sampling setup results in substantial folding-count ($M = 318, N = 455$), where previous approaches cannot handle. HoD-FP algorithm successfully reconstruct the input signal, showcasing its practical advantages of processing large amount of folds in low-sampling-rate, high-bandwidth scenarios.

IV. Conclusion

The Unlimited Sensing Framework (USF) breaks the bottleneck of concurrent high-dynamic-range and high-digital-resolution data capture in the conventional sampling scheme. In this paper, we propose a joint time-Fourier domain method that is theoretically guaranteed and offers superior performance. We benchmark our method against state-of-the-art approaches and demonstrate its superior performance in challenging hardware experiments. Our future work lies in the fronts of: (i) relaxing the sampling conditions via optimization scheme, (ii) involving the non-Gaussian measurement distortion in noise analysis and (iii) robust algorithm design.

References

[1] A. Bhandari, F. Krahmer, and R. Raskar, "On unlimited sampling," in *Intl. Conf. on Sampling Theory and Applications (SampTA)*, Jul. 2017.

[2] ——, "On unlimited sampling and reconstruction," *IEEE Trans. Sig. Proc.*, vol. 69, pp. 3827–3839, Dec. 2020.

[3] A. Bhandari, F. Krahmer, and T. Poskitt, "Unlimited sampling from theory to practice: Fourier-Prony recovery and prototype ADC," *IEEE Trans. Sig. Proc.*, pp. 1131–1141, Sep. 2021.

[4] D. Florescu, F. Krahmer, and A. Bhandari, "The surprising benefits of hysteresis in unlimited sampling: Theory, algorithms and experiments," *IEEE Trans. Sig. Proc.*, vol. 70, pp. 616–630, Jan. 2022.

[5] Y. Zhu and A. Bhandari, "Unleashing dynamic range and resolution in unlimited sensing framework via novel hardware," in *2024 IEEE SENSORS*. IEEE, Oct. 2024, pp. 1–4.

[6] S. Mulleti, E. Reznitskiy, S. Savariego, M. Namer, N. Glazer, and Y. C. Eldar, "A hardware prototype of wideband high-dynamic range analog-to-digital converter," *IET Circuits, Devices&Amp; Systems*, vol. 17, no. 4, pp. 181–192, Jun. 2023.

[7] T. Feuillen, B. S. M. R. Rao, and A. Bhandari, "Unlimited sampling radar: Life below the quantization noise," in *IEEE Intl. Conf. on Acoustics, Speech and Signal Processing (ICASSP)*, Jun. 2023.

[8] M. Beckmann, A. Bhandari, and M. Iske, "Fourier-domain inversion for the modulo Radon transform," *IEEE Trans. Comput. Imaging*, vol. 10, pp. 653–665, Apr. 2024.

[9] Z. Liu, A. Bhandari, and B. Clerckx, "λ-MIMO: Massive MIMO via modulo sampling," *IEEE Trans. Commun.*, pp. 6301 – 6315, Nov. 2023.

[10] ——, "Full-duplex beyond self-interference: The unlimited sensing way," *IEEE Communications Letters*, vol. 29, no. 1, pp. 165–169, Jan. 2025.

[11] R. Guo, Y. Zhu, and A. Bhandari, "Sub-Nyquist USF spectral estimation: K frequencies with $6K+4$ modulo samples," *IEEE Trans. Sig. Proc.*, vol. 72, pp. 5065–5076, 2024.

[12] V. Pavlíček and A. Bhandari, "Gesture recognition with USF-radars: Modulo pre-processing enhances classification," in *2025 IEEE Radar Conference (in press)*, 2025.

[13] R. Guo and A. Bhandari, "ITER-SIS: Robust unlimited sampling via iterative signal sieving," in *IEEE Intl. Conf. on Acoustics, Speech and Signal Processing (ICASSP)*, Jun. 2023.

[14] S. Rudresh, A. Adiga, B. A. Shenoy, and C. S. Seelamantula, "Wavelet-based reconstruction for unlimited sampling," in *IEEE Intl. Conf. on Acoustics, Speech and Signal Processing (ICASSP)*. IEEE, Apr. 2018, pp. 4584–4588.

[15] S. B. Shah, S. Mulleti, and Y. C. Eldar, "Lasso-based fast residual recovery for modulo sampling," in *IEEE Intl. Conf. on Acoustics, Speech and Signal Processing (ICASSP)*. IEEE, Jun. 2023.

[16] E. Romanov and O. Ordentlich, "Above the Nyquist rate, modulo folding does not hurt," *IEEE Signal Process. Lett.*, vol. 26, no. 8, pp. 1167–1171, Aug. 2019.

[17] A. Eamaz, K. V. Mishra, F. Yeganegi, and M. Soltanalian, "UNO: Unlimited sampling meets one-bit quantization," *IEEE Trans. Signal Process.*, vol. 72, pp. 997–1014, 2024.

[18] W. P. Zhang and X. Tong, "Noise modeling and analysis of SAR ADCs," *IEEE Trans. VLSI Syst.*, vol. 23, no. 12, pp. 2922–2930, Dec. 2015.

[19] R. Guo and A. Bhandari, "USF spectral estimation: Prevalence of Gaussian Cramér-Rao bounds despite modulo folding," in *2025 IEEE Statistical Signal Processing Workshop*. arXiv, 2025.

[20] S. Kay and S. Marple, "Spectrum analysis—a modern perspective," *Proc. IEEE*, vol. 69, no. 11, pp. 1380–1419, 1981.

[21] P. Stoica and A. Nehorai, "MUSIC, maximum likelihood, and Cramér-Rao bound," *IEEE Trans. Acoust., Speech, Signal Process.*, vol. 37, no. 5, pp. 720–741, May 1989.

[22] T. Blu, P.-L. Dragotti, M. Vetterli, P. Marziliano, and L. Coulot, "Sparse sampling of signal innovations," *IEEE Signal Process. Mag.*, vol. 25, no. 2, pp. 31–40, Mar. 2008.

[23] Y.-X. Yao and S. Pandit, "Cramer-Rao lower bounds for a damped sinusoidal process," *IEEE Trans. Sig. Proc.*, vol. 43, no. 4, pp. 878–885, Apr. 1995.

[24] R. Guo, Y. Li, T. Blu, and H. Zhao, "Vector-FRI recovery of multi-sensor measurements," *IEEE Trans. Sig. Proc.*, vol. 70, pp. 4369–4380, 2022.

[25] Y. Hua and T. Sarkar, "Matrix pencil method for estimating parameters of exponentially damped/undamped sinusoids in noise," *IEEE Trans. Acoust., Speech, Signal Process.*, vol. 38, no. 5, pp. 814–824, May 1990.

[26] B. N. Bhaskar, G. Tang, and B. Recht, "Atomic norm denoising with applications to line spectral estimation," *IEEE Trans. Sig. Proc.*, vol. 61, no. 23, pp. 5987–5999, Dec. 2013.